Asia-Pacific Journal of Atmospheric Sciences (2020) 56:17–28
https://doi.org/10.1007/s13143-019-00123-y

Online ISSN 1976-7951
Print ISSN 1976-7633

ORIGINAL ARTICLE

A Critical Role of Extreme Atlantic Windstorms in Arctic Warming

Ja-Young Hong [1] · Baek-Min Kim [1,2] · Eun-Hyuk Baek [1,3] · Joo-Hong Kim [1] · Xiangdong Zhang [4] · Seong-Joong Kim [5]

Received: 20 October 2018 / Revised: 14 April 2019 / Accepted: 16 April 2019 / Published online: 2 May 2019

Abstract

Here we show that Atlantic windstorms of extreme category in northern winter tend to follow a well-defined route toward the Atlantic sector of Arctic, and that heat and moisture transported by these extreme storms significantly warm the Arctic. A positive North Atlantic Oscillation (NAO) condition and the associated intensified upper-level Atlantic jet provide favorable conditions for those extreme storm developments through enhanced vertical wind shear. These extreme windstorms lead to two discernible impacts on the Arctic: 1) enhanced poleward energy transport by moisture intrusion to the Arctic, which accompanies increased longwave downward radiation and 2) the occurrence of blocking-like patterns after the storm break-up. During these periods, significant Arctic warming was observed of a 10-fold increase versus normal and weak storms. The poleward deflections of extreme storms, and the Arctic warming driven by such storms, are well simulated in numerical experiments with ocean-atmosphere coupled models.

Keywords Atlantic windstorm · Arctic warming · Extreme windstorm · Storm intensity

1 Introduction

Since the 1950s, the Arctic surface and even lower tropospheric temperature has increased, at a rate almost twice the global mean (approximately 0.12 °C per decade), a phenomenon known as Arctic amplification (IPCC 2007a, 2013). Arctic warming is most pronounced during winter (IPCC 2007b) resulting from a combination of several significant factors, including increased greenhouse gas concentrations (Gillett et al. 2008; Stroeve et al. 2012) and positive feedbacks related to snow and sea ice (Winton 2006; Screen et al. 2012), aerosol and black carbon (Shindell and Faluvegi 2009), cloud cover and water vapor (Francis and Hunter 2006; Graversen and Wang 2009), surface thermal inversion (Bintanja et al. 2011), and atmospheric lapse rates (Pithan and Mauritsen 2014). In addition to these local sources, Arctic warming is also strongly linked with wave-induced poleward energy transport at both the planetary scale and synoptic scale (Graversen et al. 2008; Lee 2014; Park et al. 2015b; Woods and Caballero 2016; Baggett and Lee 2017; Luo et al. 2017).

The importance of poleward atmospheric energy transport in explaining polar or Arctic amplification has been suggested as mentioned above, even in a system without snow- or ice-albedo feedback (Flannery 1984; Alexeev et al. 2005; Alexeev and Jackson 2013). Atmospheric heat from the lower latitudes is transported to the high Arctic by either large-scale circulation or synoptic-scale cyclones. In the literature, a number of studies focused on the storm

Responsible Editor: Soon II An.

Electronic supplementary material The online version of this article (https://doi.org/10.1007/s13143-019-00123-y) contains supplementary material, which is available to authorized users.

✉ Baek-Min Kim
baekmin@pknu.ac.kr

[1] Unit of Arctic Sea-Ice Prediction, Korea Polar Research Institute, Incheon, South Korea

[2] Department of Environmental Atmospheric Sciences, Pukyong National University, Busan, South Korea

[3] Faculty of Earth and Environmental Sciences, Chonnam National University, Gwangju, South Korea

[4] International Arctic Research Center and Department of Atmospheric Sciences, University of Alaska Fairbanks, Fairbanks, AK, USA

[5] Division of Polar Climate Sciences, Korea Polar Research Institute, Incheon, South Korea

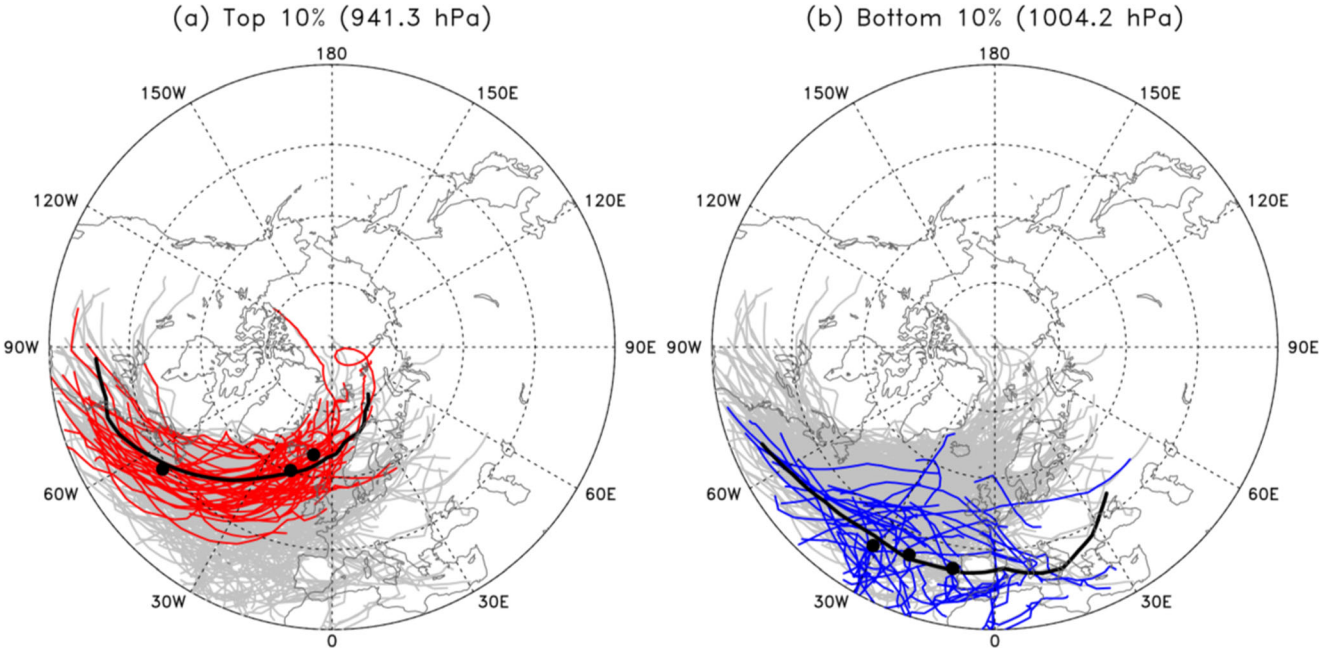

Fig. 1 Atlantic windstorm tracks classified according to maximum intensity (i.e., minimum central pressure) of each windstorm. In total, there are 591 Atlantic windstorms detected in the winters of 1981–2016, and each extreme (top 10% and bottom 10%) storm case includes 59 of these storms. The gray, red, blue, and black lines, respectively, indicate the tracks of total, **a** strong, **b** weak storms, and their mean paths. The black dots in sequence from left to right are the mean locations of cyclogenesis, the maximum intensity step, and cyclolysis, respectively. The numbers in parentheses above each figure are the averaged minimum central pressures

generated inside the Arctic basin and found that the number of Arctic cyclones are increasing and they play important role in Arctic warming (Zhang et al. 2004; Orsolini and Sorteberg 2009; Simmonds and Rudeva 2014; Rinke et al. 2017). However, the role of mid-latitude synoptic-scale storms in Arctic warming is still unclear. In this circumstance, recent Atlantic winter storm intrusion event that significantly contributed to the unprecedented Arctic warming of 2016 provides us an invaluable opportunity to examine the relationship (Kim et al. 2017). A recent study showed that the transient eddies, considerably associated with synoptic storms, are responsible for about 90% of all moisture transport into the Arctic (Dufour et al. 2016).

On the other hand, Arctic warming exhibits a systematic development pattern – a low over the Arctic Basin and a high over northern Eurasia – helping to generate a favorable pathway for moisture intrusion into the Arctic (Overland and Wang 2010; Zhang et al. 2013; Messori et al. 2018). Intense moisture intrusions across 70°N latitude exerts considerable control over polar temperatures, and their trajectories are concentrated in the Atlantic sector (Woods et al. 2013; Woods and Caballero 2016).

Although several previous studies have suggested the critical role of extreme heat and moisture intrusion into the Arctic for recent Arctic amplification, still no studies explicitly point out the specific physical mechanism on how atmospheric waves carry the pack of large energy into the Arctic from outside. Here, we specifically focused on the role of extratropical cyclones and chased every single storm that occurred Atlantic Ocean during winter over a 36-year period (December–January-February 1981/82–2016/17) by storm detection and tracking techniques. For this, we classify North Atlantic windstorms according to their storm intensities (i.e., minimum central pressures) and explore their relationship to Arctic temperature and atmospheric circulation changes, particularly in the Atlantic side of the Arctic Ocean.

2 Data and Methods

We used the Japanese 55-year reanalysis data (Kobayashi et al. 2015) over 36 winter seasons (December to February) for the period 1981–2017. The data have a 6-hly temporal resolution and a 1.25° horizontal resolution. Anomalies are calculated based on the 30-yr climatological mean for the

Fig. 2 Atmospheric states at the initial stage of the strong storms. Daily ▶ composites of anomalous (**a**) sea level pressure, (**b**) 300-hPa zonal wind, (**c**) Eady growth rate between 200 and 850 hPa, and (**d**) surface air temperature on the cyclogenesis dates of the top 10% of storms. The black dots are mean cyclogenesis locations for the top 10% strong storms. Only values exceeding the 10% significance level of a *t* test are hatched

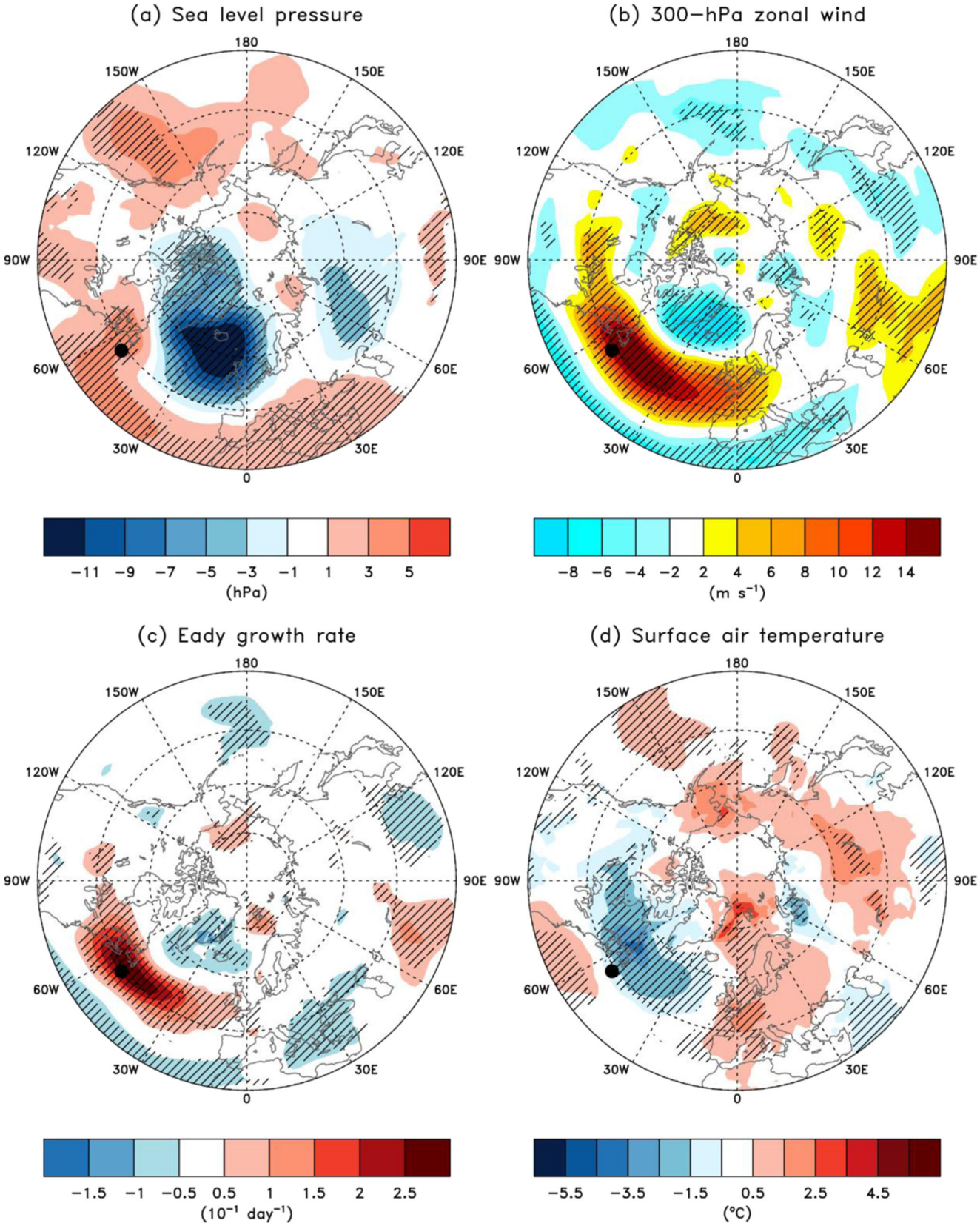

period 1981–2010. The significance of the observed and modeled data is evaluated based on a two-tailed Student's *t* test, and the confidence intervals are detailed in the figure captions. The Eady growth rate between 200 and 850 hPa is

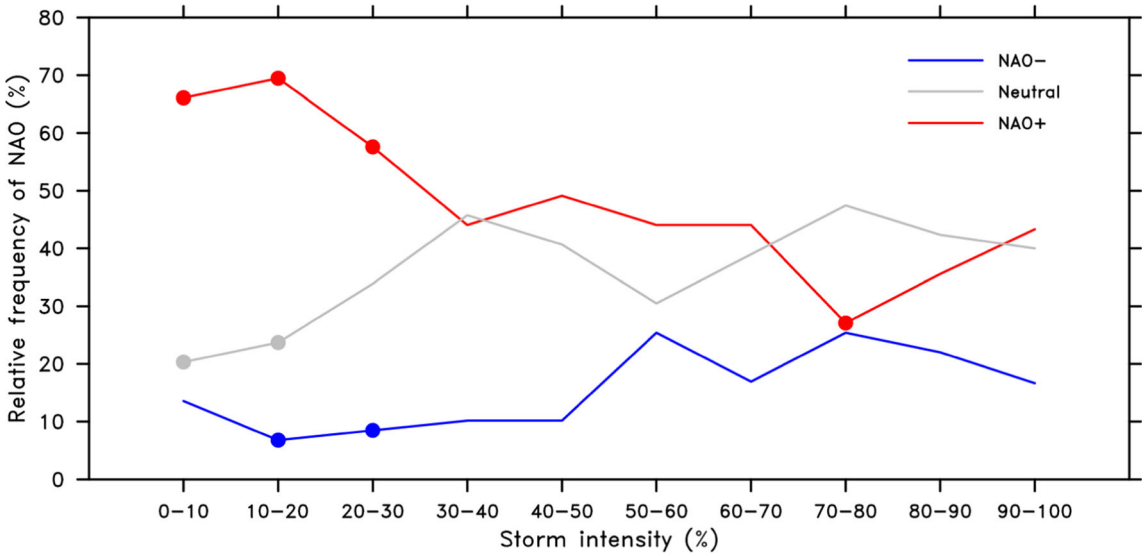

Fig. 3 Relative NAO frequency (in % of days) of each storm intensity at the storm genesis date. A daily NAO index (NAOI) provided by the National Oceanic Atmospheric Administration Climate Prediction Center (ftp://ftp.cpc.ncep.noaa.gov/cwlinks/). The index is constructed by projecting daily 500-hPa geopotential height anomalies onto the NAO loading pattern (Barnston and Livezey 1987) obtained for analyzing NAO variability. The NAO phases are divided into three subsets: (1) NAO+ (NAOI ≥ +0.5); (2) Neutral (−0.5 < NAOI < +0.5); and (3) NAO- (NAOI ≤ −0.5). The colored dots indicate statistical significant at the 5% significance level of a Monte Carlo test that generated bootstrapped samples of composite patterns from 10,000 random samples. Each sample composite was calculated with N randomly selected daily anomalies, where N is the number of matching days for a particular storm case ($N = 59$ for the top 10% to 80–90% case and 60 for the bottom 10% (90–100%))

used as an indicator of baroclinic instability; a detailed description can be found in Kim et al. (2017). To analyze water vapor transport, the vertically integrated moisture flux was estimated as follows:

$$\boldsymbol{Q} = -\frac{1}{g}\int_{P_{sfc}}^{P_{top}} q\boldsymbol{V}\, dp$$

where g is the gravitational constant, q is specific humidity, $\boldsymbol{V}$ is the horizontal wind vector, dp is the change in pressure, P_{sfc} is the surface pressure, and P_{top} is the pressure at the top of the atmosphere. In this study, 300 hPa is regarded as the top of the atmosphere because the amount of water vapor above 300 hPa is considered negligible (Kobayashi et al. 2015).

In order to investigate the impacts of extreme Atlantic windstorms on Arctic warming, we conducted two distinct fully-coupled ocean-atmosphere climate model experiments using present-day aerosol emissions forcing and initial conditions. One model used in this study was the Climate Model version 2.1 (CM2.1) developed by the Geophysical Fluid Dynamical Laboratory (Delworth et al. 2006), integrated over 100 years with 2° latitude × 2.5° longitude horizontal resolution and 24 vertical levels. The other is the Community Earth System Model (CESM) version 1.2.2 of the National Center for Atmospheric Research, integrated over 100 years with 1.9° latitude × 2.5° longitude horizontal resolution and 26 vertical levels, and using Community Atmospheric Model version 4 physics.

The storm detection and tracking method used in this study is a modified version of Vitart et al. (1997). The criteria specifically applied to tropical storm detection were disabled so that the method can best capture the Northern Hemisphere extratropical storms. Thus, our detection of extratropical storms was based on the relative vorticity at 850 hPa and the mean sea level pressure. This method comprises the procedures of detecting storm center candidates and of tracking the moving center of a given storm over time.

First, the detection procedure of storm center candidates follows these steps:

1) A local maximum of the 850-hPa relative vorticity larger than 2.0×10^{-5} s^{-1} is found in each 11 × 11 grid window.
2) The closest local minimum of the mean sea level pressure is found within a 400 km radius of the local vorticity maximum.
3) The mean sea level pressure should increase by at least 15 Pa in all directions within a 500 km distance from the local pressure minimum.
4) The equatorward limit of detection is set at 30°N for Northern Hemisphere extratropical storms.

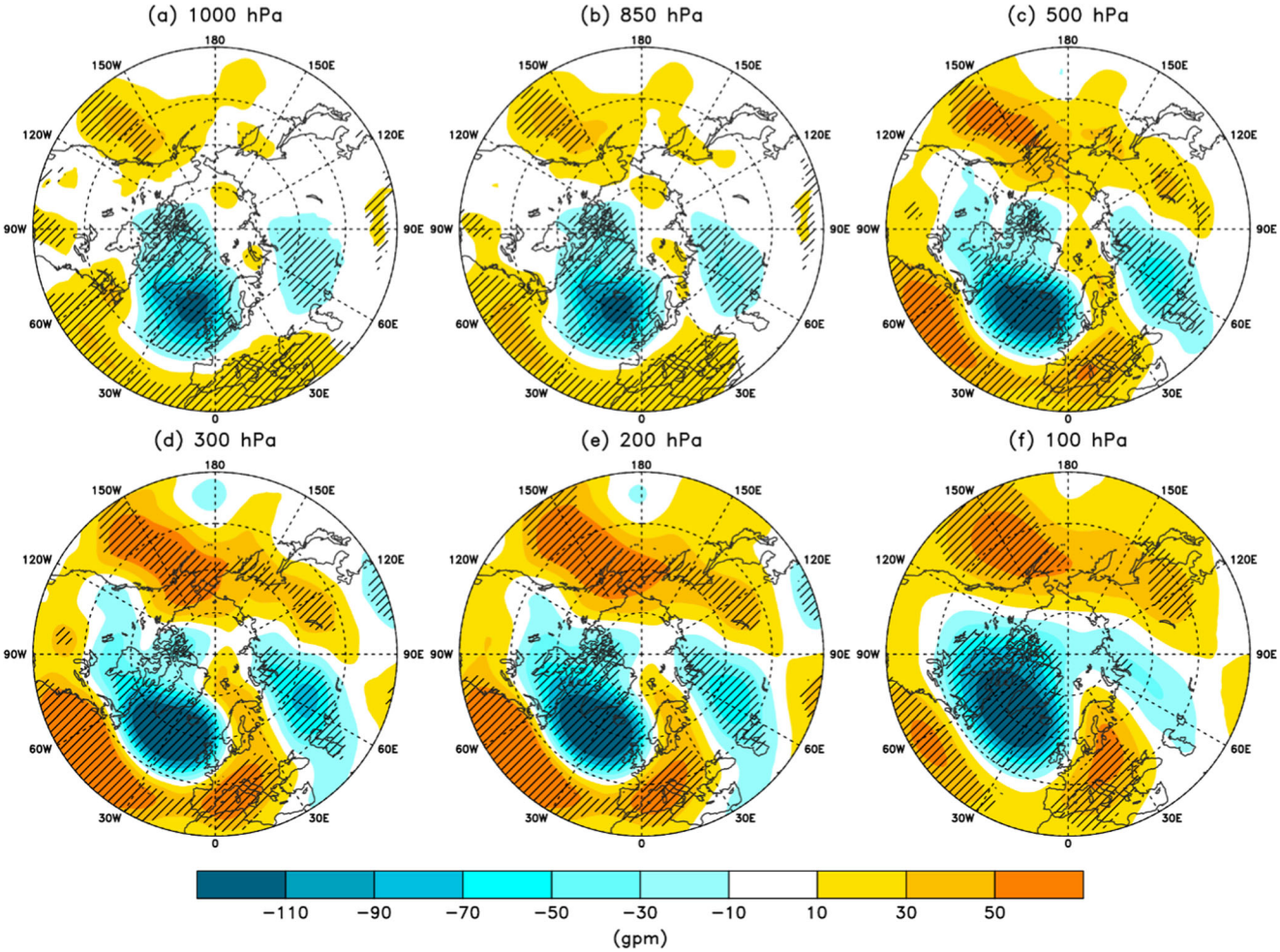

Fig. 4 Initial geopotential state of the strongest storms. Daily composites of anomalous geopotential height at (**a**) 1000 hPa, (**b**) 850 hPa, (**c**) 500 hPa, (**d**) 300 hPa, (**e**) 200 hPa, and (**f**) 100 hPa on the cyclogenesis dates of strong storms. Only values exceeding the 10% significance level of a *t* test are hatched

Next, the tracking procedure was applied to connect the detected 6-hourly storm center candidates and generate the full life-cycle for each storm. Given the 6-hourly data, the tracking procedure was comprised of technical steps to effectively detect the most probable next position six hours later. The tracking procedure is summarized as follows:

1) For a given storm, a circular tracking boundary with a 750 km radius is set at each 6-hourly time step, and the location of the storm at that time step is set as the center of the circle. Then, the storm centers at the next time step are examined within the boundary.
2) If one storm center is found within the boundary, it is determined as the next storm position. In case of multiple storm centers, priority is given to the closest storm center located in the front half of the circle, towards the direction of the storm's movement. If there is no such storm center at the front half of the circle, the closest one is selected as the next position. If no storm appears within the boundary, the tracking of that given storm stops.
3) Finally, only storms with lifetimes equal to or greater than 1.5 days are considered.

For investigation how atmospheric variables influence the Arctic warming, the lead–lag relationships are constructed by calculating composites of the various projection time series where the lag-0 days are defined as those days when the strong storms terminated. The time evolution can be examined effectively using a daily projection time series (Feldstein 2002) that measures how closely the atmospheric variable anomalies, at any given day, resemble the each

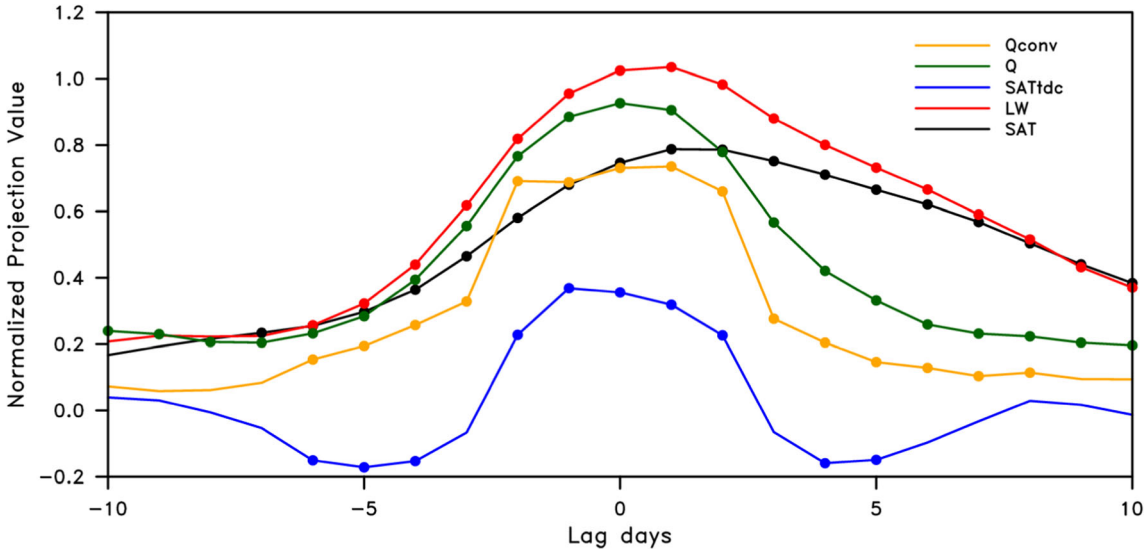

Fig. 5 5-day running-mean lag-day composites of SAT (black), surface downward longwave radiation (LW, red), SAT tendency (blue), moisture (dark green), and moisture convergence (orange) projection time series. Filled dots indicate statistical significance at the 10% significance level, evaluated with a Monte Carlo method where the composite values were compared against 10,000 randomly selected samples

variable trend pattern. A detailed projection description can be found in Park et al. (2015a).

3 Results

To investigate the existence of a systematic difference in windstorm tracks depending on storm intensity (defined as minimum central pressure), we conducted a percentile analysis. Each Atlantic windstorm is binned into 10 consecutive percentiles. Figure 1 shows all storm trajectories in the top 10% (A; red curves) and bottom 10% (B; blue curves) during the 36 winter seasons.

As clearly shown in Fig. 1a, the storms in the top 10% category exhibit similar trajectories to one another as compared to the bottom 10% category, directing more poleward toward the Atlantic Arctic sector. In the top 10% of storms, trajectories tend to be confined to the Greenland Sea before their extinction. In contrast, in the bottom 10% category, the storms are mostly spread over lower latitudes (30°N–60°N), and the average path passes zonally throughout Western Europe. Individual paths also differ greatly from one another. The strongest 10% of storms tend to originate over the western North Atlantic Ocean just to the east of North America coast, where there is a strong oceanic front produced by the poleward Gulf Stream warm water and the equatorward Labrador cold water current. On the contrary, the weakest 10% of storms depicted in Fig. 1b originate in the middle of the Atlantic Ocean. A close examination indicates that the averaged locations of strong storm centers at the maximum intensity and cyclolysis stages, the processes by which cyclones weaken and terminate, (the middle and right-most black dots in Fig. 1a and b) of the strongest (weakest) are located more northward (eastward) towards the Arctic (Western Europe). Complete information on the 10th percentile trajectories is provided in Supplementary Information (Fig. S1), confirming that the stronger (weaker) the intensity, the more poleward (eastward) the storm tracks tend to be aligned.

The composites of atmospheric variables for the top 10% strong storms on their initial (cyclogenesis) dates defined as the first dates of each storm detection are shown in Fig. 2. The anomalous sea level pressure (Fig. 2a) over Iceland/southern Greenland (negative) and eastern North America (positive) indicates a deepening of the Icelandic Low and a strengthening of the Azores High, respectively. This pattern shows a strong projection on to positive North Atlantic Oscillation (NAO). Further analysis suggests that strong storms generally occur with positive phase NAO (Fig. 3). The NAO-like patterns at the initial stage of the strong storm development exhibits a barotropical structure (Fig. 4). This pattern increases the meridional pressure gradient between the Icelandic Low and Azores High regions. Thus, an accelerated 300-hPa zonal wind (Fig. 2b) with a maximum of approximately 14 m s^{-1} occurs over the North Atlantic, especially in the cyclogenesis region. In association with these anomalous pressure and zonal wind patterns, positive Eady growth rates (Fig. 2c) that represent intensified baroclinic instability are centered in the regions of the enhanced westerly jets. The composite also shows greatest surface air temperature (SAT) gradients over the northwestern Atlantic (Fig. 2d). Therefore, both the surface thermal condition and the large-scale circulation settings are highly

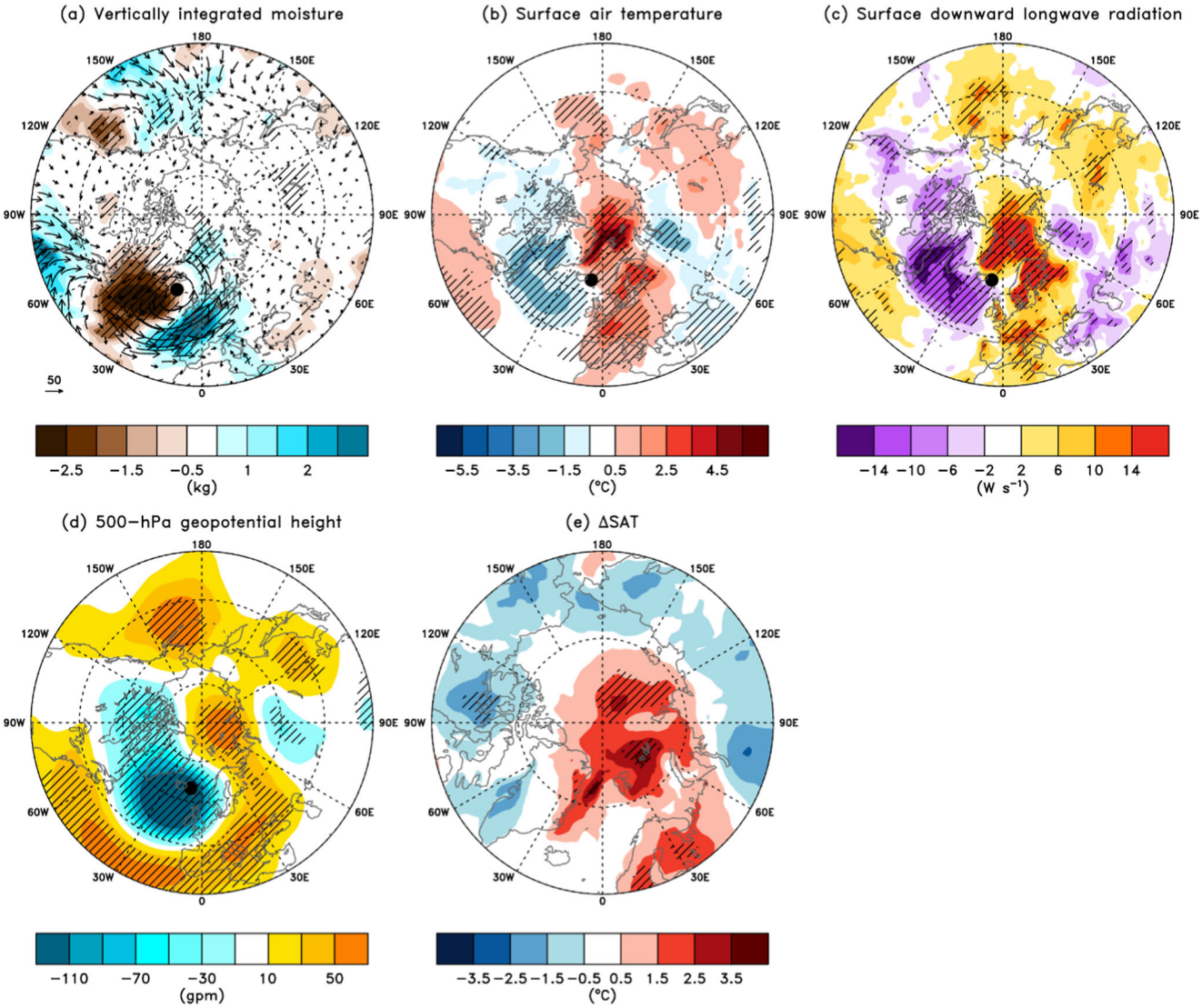

Fig. 6 Atmospheric states at peak and dissipation stages of the strong storms. The same as Fig. 2, but for (**a**) vertically integrated horizontal moisture flux (arrows) and its convergence (shading) on the peak dates of strong storms; **b** surface air temperature, **c** surface downward longwave radiation, and (**d**) 500-hPa geopotential height on cyclolysis dates of strong storms; and (**e**) temperature difference (tendency) between cyclolysis and cyclogenesis dates. The black dots are average locations of cyclolysis

favorable for cyclogenesis over the northwestern North Atlantic (Chang et al. 2002).

Figure 5 shows that surface downward longwave radiation fluctuations are almost coincide with the vertically integrated moisture into the Arctic until strong storms are terminated. After the strong storm terminations, moisture influx is followed shortly by an increase in surface downward longwave radiation (Park et al. 2015a). The SAT variances are preceded by an increase in surface downward longwave radiation and tropospheric moisture and its flux convergence.

The influx of moisture from the Atlantic sector is an important source for winter Arctic amplification (Woods et al. 2013; Park et al. 2015b; Woods and Caballero 2016; Kim et al. 2017). The strengthened vertically integrated moisture flux (arrows in Fig. 6a) enters intensely from the North Atlantic to the Arctic and curves cyclonically, while an anti-cyclonic

Table 1 The change in surface air temperature. The temperature is averaged over the Barents-Kara Seas (75°-90°N, 0°-90°E) between cyclolysis and cyclogenesis dates (ΔSAT) at each storm intensity level. An asterisk denotes statistical significance at the 1% significance level of a *t* test

Top (%)	10	10–20	20–30	30–40	40–50	50–60	60–70	70–80	80–90	90–100
Mean (°C)	2.02*	0.21	0.22	0.18	−0.53	−0.68	0.04	−0.70	−0.89	−0.42

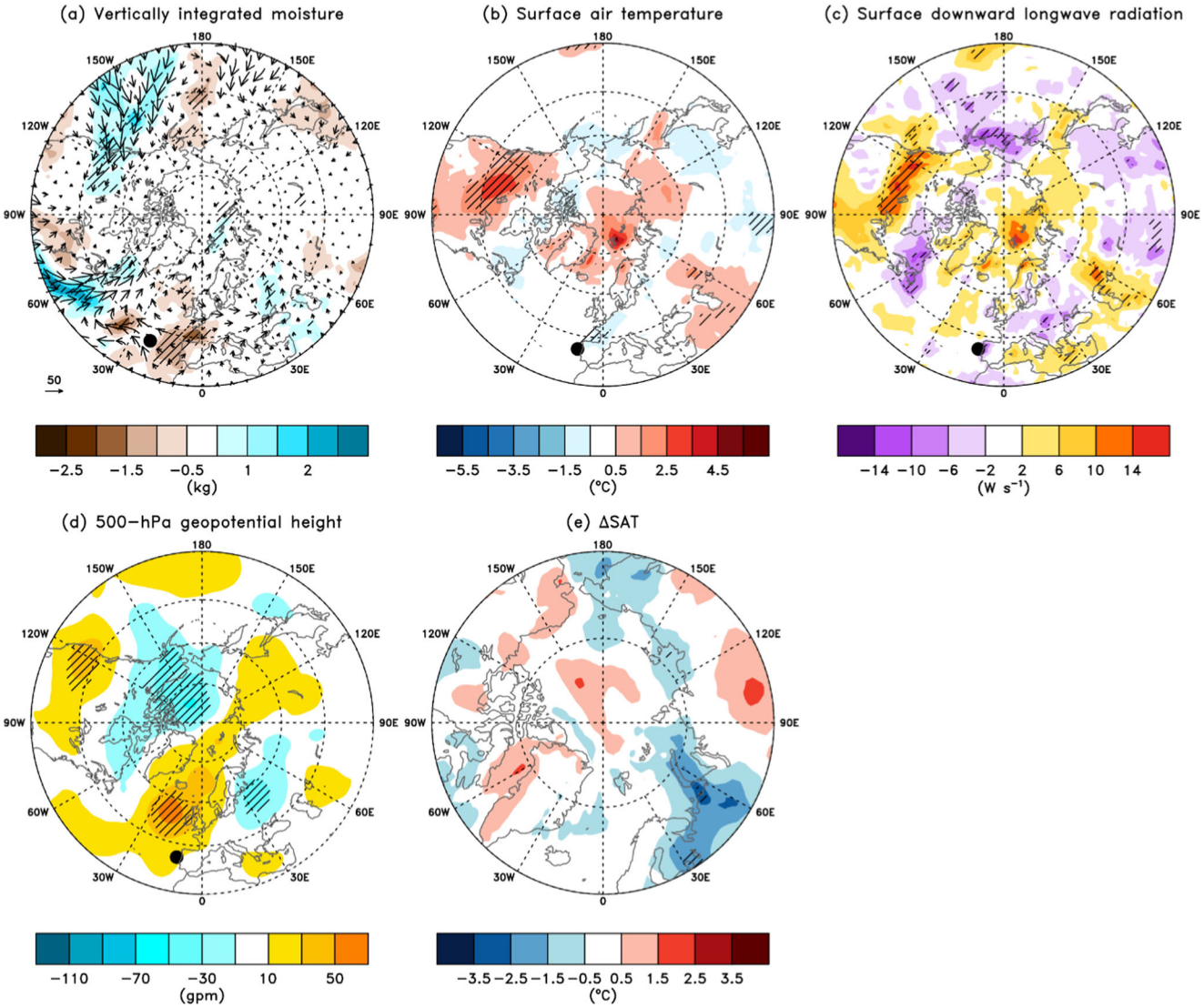

Fig. 7 Same as Fig. 6, but for weak storms

circulation appears over the western North Atlantic on the peak dates of strong storms. Consistent with this anomalous fluxes, the moisture convergence (shading in Fig. 6a) is positive (negative) in Northern Europe along 0°E (North Atlantic along 330°E). These strong moisture injections to the Arctic by strong storms contribute to Arctic warming of up to 3 °C, particularly in the Barents-Kara seas on the cyclolysis date (Fig. 6b). This weakens the surface temperature inversion over the Arctic Ocean and promotes thermodynamic instability by changes in the lapse rate (Woods and Caballero 2016; Kim et al. 2017). Surface downward longwave radiation is positive in the region where the surface warming is increased by moisture and clouds (Fig. 6c). The spatial structure of the radiation anomaly is considerably similar to that of the SAT anomaly, with a pattern correlation of 0.90. Corresponding to the anomalous moisture convergence, there is positive (negative) anomalies of 500 hPa geopotential height (Fig. 6d) over Northern Europe and the Barents-Kara seas. The positive pattern indicates the occurrence of European blocking after the dissipation of strong storms (Michel et al. 2012; Luo et al. 2014; Kim et al. 2017). The change in SAT between cyclolysis and cyclogenesis dates (ΔSAT) clearly increases over Northern Europe and the Barents-Kara seas (Fig. 6e). The analysis here therefore suggest that strong storms induce a moisture convergence and, in turn, an increase in surface downward longwave radiation, contributing to Arctic warming. The area-averaged ΔSAT over the Barents-Kara seas is about 2.0 °C, statistically significant at the 1% significance level (Table 1).

Different from the strong storms, the moisture anomaly decrease over the Atlantic sector of the Arctic and increase over the northwestern Atlantic when the weakest storms are active (Fig. 7a). On the termination dates of the weakest storms, increase in SAT (Fig. 7b) over the

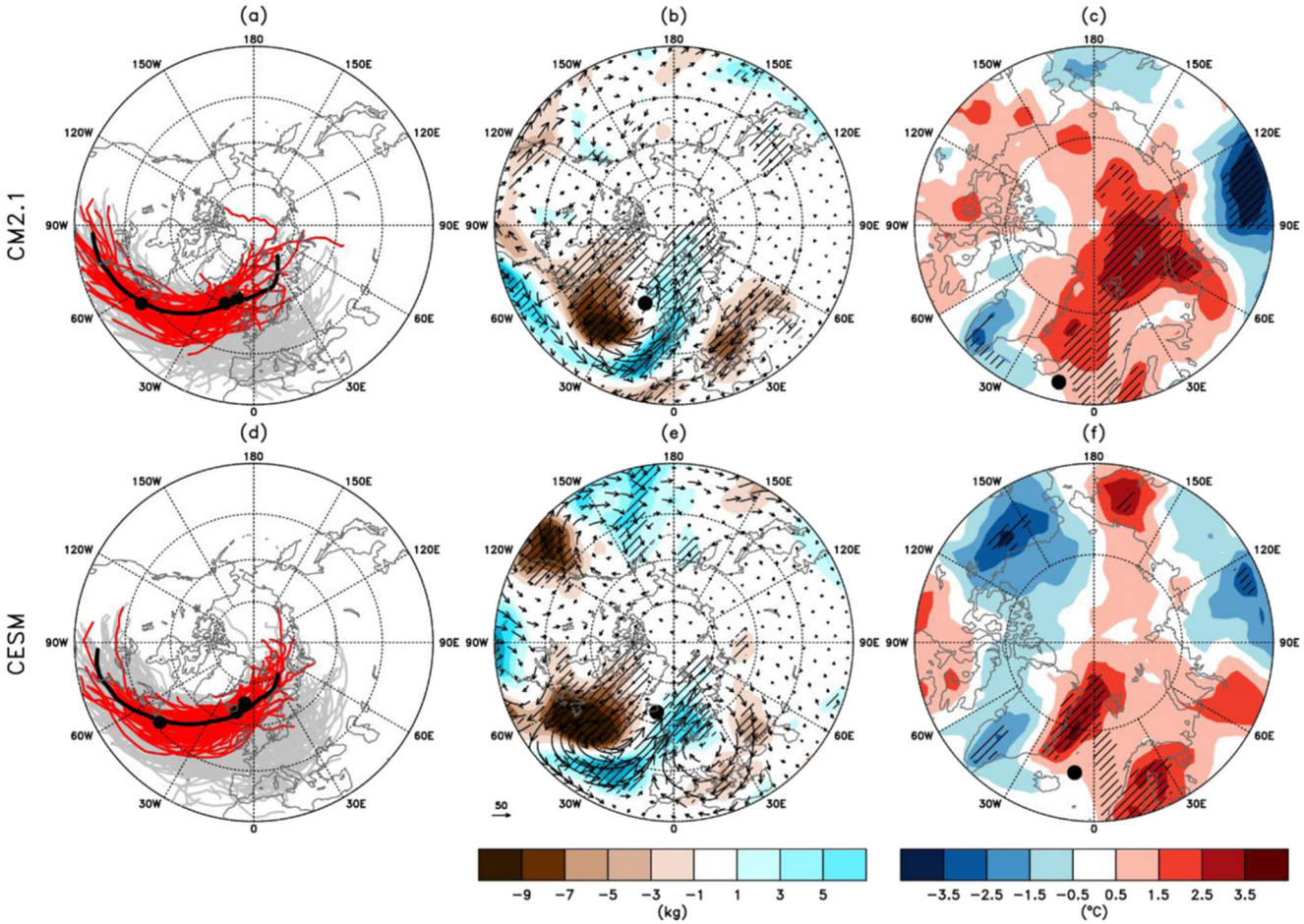

Fig. 8 Simulated characteristics of the top 10% of Atlantic windstorms. The same as in Fig. 1a, but for (**a**) CM2.1 and (**d**) CESM. The detected number of Atlantic windstorms for 100 winters of CM2.1 and CESM is 911 and 922, respectively. The averaged minimum central pressures of the top of 10% storms of CM2.1 and CESM are 944.4 hPa and 939.7 hPa, respectively. The same as in Fig. 6a, but for (**b**) CM2.1 and (**e**) CESM. The same as in Fig. 6e, but for (**c**) CM2.1 and (**f**) CESM

Barents-Kara Seas is likely relevant to blocking (positive anomaly, Fig. 7d) rather than driven by storms. However, this increase is not significant and ΔSAT has nothing distinctive over the Barents-Kara Seas (Fig. 7e). Compare to the strong storms, weak storms rarely help the Arctic warming according to weak moisture intrusion.

The characteristics of the top 10% of storms and their contribution to Arctic warming were also investigated using model outputs from two different coupled climate models, all of which were forced with present-day aerosol emissions forcing and initial conditions. The number of the top 10% strong storms for 100 winters in the CM2.1 (Fig. 8a) and CESM (Fig. 8d) simulations are 91 and 92, respectively. Their mean central pressures have approximately the same value as the observed storms. The storms traversing 60°N in CM2.1 are more widely spread than those in CESM, but the Atlantic storm trajectories clearly tilt northeastward toward the Arctic in both model results. The observational analysis suggests that moisture intrusion is an important driver of warming in the Barents-Kara seas. On the peak dates of the top 10% strong storms, the influx of warm moist air from the North Atlantic is obvious between Greenland and Svalbard (arrows in Fig. 8b and e) where the moisture convergence reaches its maximum (shading in Fig. 8b and e). This is consistent with the observation shown in Fig. 6a. In agreement with the increased moisture convergence, positive ΔSAT occurs in the simulations over the Atlantic sector of the Arctic and the Barents-Kara seas (Fig. 8c and f). This is the same as that in the observational analysis. A quantitative analysis indicates that the warming induced by the top 10% of storms in CM2.1 (CESM) is 2.5 °C (1.3 °C), significant at the 1% (5%) significance level. Therefore, the model results reinforce the observational analysis results with a greatly increased sample size of strong storms, suggesting the importance of moist air

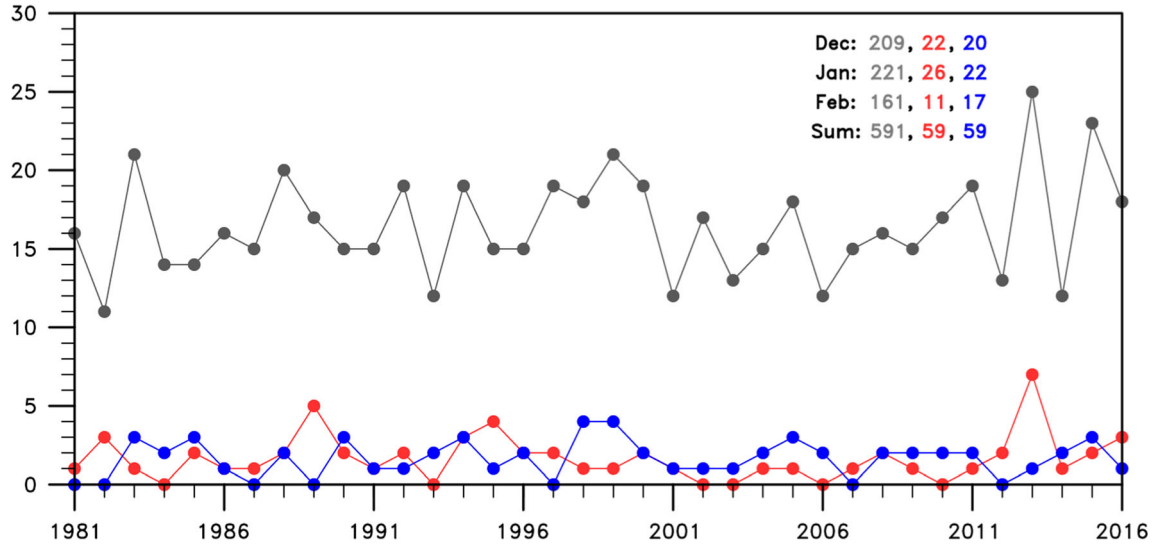

Fig. 9 Time series of the total (gray), strong (red), and weak (blue) number of Atlantic windstorms for 36 winters. The total number of storms is 591, and $N = 59$ for both the strong and weak windstorm categories. The numerals in the figure, respectively, are the number of occurrences of the total, strong, and weak storms in December, January, February, and their summation

transport by extreme Atlantic windstorms for extreme warming over the Barents-Kara seas in boreal winters.

4 Summary and Discussion

In this study, the statistical relationship between warming events in the Arctic and extreme Atlantic windstorms was investigated in detail using a 36-winter record of six-hourly extratropical windstorm statistics computed for the Northern Hemisphere. Windstorm locations and characteristics were obtained by applying the modified Vitart et al. (1997) algorithm to 850-hPa relative vorticity and sea level pressure at 6-hour intervals.

When examining trajectories of storms for every 10th percentile of storm intensity, we found that the stronger Atlantic windstorms tend to move northeastward to the Atlantic sector of Arctic Ocean, while weaker storms tend to move eastward towards Western Europe. This tendency is much more robust for extreme Atlantic windstorms, i.e., the highest 10th percentile, providing a sufficient motivation for detailed examination on the role of extreme Atlantic windstorms on the Arctic warming events. The dynamic mechanisms for the poleward deflection of stronger storms have been found to be similar to those for cyclone development in general, such as the potential vorticity (PV) interaction between the upper- and low-levels and the diabatic heating by latent heat release (Tamarin and Kaspi 2016). The higher PV at the upper-level trough, which is located to the west of the low-level cyclone, induces poleward meridional velocity of the low-level cyclone primarily by the nonlinear advection. The diabatic heating by poleward-moving and ascending warm and moist air at the northeastern side of the cyclone also exerts influence on the poleward movement of the low-level cyclone. Therefore, in accordance with the previous study, we suggest that higher baroclinic environment depicted at the initial stage of the extreme Atlantic windstorms (Fig. 2d) is conducive precondition for the poleward movement of the extreme Atlantic windstorms.

Composite analyses show that the top 10% of storms develop under a positive NAO pattern, associated with an enhanced jet stream and baroclinicity, and an increased meridional temperature gradient over the North Atlantic, supporting previous findings (Luo et al. 2017; Donat et al. 2010; Pinto and Raible 2012; Gómara et al. 2014). In accordance with previous studies, we found that anomalous moisture transport into the Arctic during a storm's lifetime is important for Arctic warming, particularly for the Barents-Kara seas. After the break-up of top 10% storms, an increase in surface downward longwave radiation is observed over the Atlantic sector of the Arctic and Barents-Kara seas. After an abrupt increase in Arctic temperatures by storm intrusion, an intensification of middle tropospheric geopotential height anomaly over Europe and near the Ural Mountains is observed, reflecting the occurrence of blocking induced by strong storms. These mechanisms contribute to the longer maintenance of warming over the Arctic, especially the Barents-Kara seas.

Through fully-coupled model simulations of current climate condition using CM2.1 and CESM, we successfully reproduced characteristics similar to the top 10% of storm

trajectories, and composite patterns similar to those observed. This finding suggests that the temperature increase of the Arctic driven by poleward energy transport of extreme Atlantic windstorms is a result of pure internal process easily simulated by contemporary current climate models. Modulation of this internal process by increase of CO_2 forcing and subsequent changes in the degree of Arctic warming can be an important issue that we are currently preparing as a future work.

Since Arctic warming has been much more pronounced over the last two decades (Serreze et al. 2009) and storm tracks shift more poleward under global warming (Tamarin and Kaspi 2017a, b), a natural question arises: Has the number of Atlantic windstorms been increasing in recent decades, supporting more pronounced Arctic warming events? In our analysis here, we found that, interestingly, there is no significant trend of the number of Atlantic windstorms in recent decades (Fig. 9). Rinke et al. (2017) showed that the trends in extreme windstorms developed at high-latitude increase in November–December and decrease in January. However, it should be noted that they only examined storms generated within the Arctic Circle. Therefore, the findings of Rinke et al. (2017) give some hints. The changed Arctic climate condition such as weakened polar jet and vertical stratification provide easier Rossby wave breaking. This condition could be a reason for the amplifying role of Atlantic storm in the Arctic warming events. We are currently under investigation on this possibility.

Acknowledgments This study was supported by 'Development and Application of the Korea Polar Prediction System (KPOPS) for Climate Change and Weather Disaster (PE19130)' project of the Korea Polar Research Institute.

References

Alexeev, V.A., Jackson, C.H.: Polar amplification: is atmospheric heat transport important. Clim. Dyn. **41**, 533–547 (2013). https://doi.org/10.1007/s00382-013-1763-3

Alexeev, V.A., Langen, P.L., Bates, J.R.: Polar amplification of surface warming on an aquaplanet in ghost forcing experiments without sea ice feedbacks. Clim. Dyn. **24**, 655–666 (2005). https://doi.org/10.1007/s00382-005-0018-3

Baggett, C., Lee, S.: An identification of the mechanisms that lead to Arctic warming during planetary-scale and synoptic-scale wave life cycles. J. Atmos. Sci. **74**, 1859–1877 (2017)

Barnston, A.G., Livezey, R.E.: Classification, seasonality, and persistence of low-frequency atmospheric circulation patterns. Mon. Weather Rev. **115**, 1083–1126 (1987)

Bintanja, R., Graversen, R.G., Hazeleger, W.: Arctic winter warming amplified by the thermal inversion and consequent low infrared cooling to space. Nat. Geosci. **4**, 758–761 (2011). https://doi.org/10.1038/ngeo1285

Chang, E.K.M., Lee, S., Swanson, K.L.: Storm track dynamics. J. Clim. **15**, 2163–2183 (2002). https://doi.org/10.1175/1520-0442(2002)015<02163:STD>2.0.CO;2

Delworth, T.L., Broccoli, A.J., Rosati, A., Stouffer, R.J., Balaji, V., Beesley, J.A., Cooke, W.F., Dixon, K.W., Dunne, J., Dunne, K.A., Durachta, J.W., Findell, K.L., Ginoux, P., Gnanadesikan, A., Gordon, C.T., Griffies, S.M., Gudgel, R., Harrison, M.J., Held, I.M., Hemler, R.S., Horowitz, L.W., Klein, S.A., Knutson, T.R., Kushner, P.J., Langenhorst, A.R., Lee, H.-C., Lin, S.-J., Lu, J., Malyshev, S.L., Milly, P.C.D., Ramaswamy, V., Russell, J., Schwarzkopf, M.D., Shevliakova, E., Sirutis, J.J., Spelman, M.J., Stern, W.F., Winton, M., Wittenberg, A.T., Wyman, B., Zeng, F., Zhang, R.: GFDL's CM2 global coupled climate models. Part I: formulation and simulation characteristics. J. Clim. **19**, 643–674 (2006). https://doi.org/10.1175/JCLI3629.1

Donat, M.G., Leckebusch, G.C., Pinto, J.G., Ulbrich, U.: Examination of wind storms over Central Europe with respect to circulation weather types and NAO phases. Int. J. Climatol. **30**, 1289–1300 (2010). https://doi.org/10.1002/joc.1982

Dufour, A., Zolina, O., Gulev, S.K.: Atmospheric moisture transport to the Arctic: assessment of reanalyses and analysis of transport components. J. Clim. **29**, 5061–5081 (2016). https://doi.org/10.1175/JCLI-D-15-0559.1

Feldstein, S.B.: Fundamental mechanisms of the growth and decay of the PNA teleconnection pattern. Quart. J. Roy. Meteor. Soc. **128**, 775–796 (2002). https://doi.org/10.1256/0035900021643683

Flannery, B.P.: Energy-balance models incorporating transport of thermal and latent energy. J. Atmos. Sci. **41**, 414–421 (1984). https://doi.org/10.1175/1520-0469(1984)041<0414:EBMITO>2.0.CO;2

Francis, J.A., Hunter, E.: New insight into the disappearing Arctic Sea ice. Eos, Trans. AGU. **87**, 509–511 (2006). https://doi.org/10.1029/2006EO460001

Gillett, N.P., Stone, D.A., Stott, P.A., Nozawa, T., Karpechko, A.Y., Hegerl, G.C., Wehner, M.F., Jones, P.D.: Attribution of polar warming to human influence. Nat. Geosci. **1**, 750–754 (2008). https://doi.org/10.1038/ngeo338

Gómara, I., Pinto, J.G., Woollings, T., Masato, G., Zurita-Gotor, P., Rodríguez-Fonseca, B.: Rossby wave-breaking analysis of explosive cyclones in the euro-Atlantic sector. Q. J. R. Meteorol. Soc. **140**, 738–753 (2014). https://doi.org/10.1002/qj.2190

Graversen, R.G., Wang, M.: Polar amplification in a coupled climate model with locked albedo. Clim. Dyn. **33**, 629–643 (2009). https://doi.org/10.1007/s00382-009-0535-6

Graversen, R.G., Mauritsen, T., Tjernström, M., Källén, E., Svensson, G.: Vertical structure of recent Arctic warming. Nature. **451**, 53–56 (2008). https://doi.org/10.1038/nature06502

IPCC: Climate change 2007: the physical science basis. In: Solomon, S., Qin, D., Manning, M., Chen, Z., Marquis, M., Averyt, K.B., Tignor, M., Miller, H.L. (eds.) Contribution of Working Group I to the Fourth Assessment Report of the Intergovernmental Panel on Climate Change. Cambridge University Press, Cambridge (2007a)

IPCC: Climate change 2007: impacts, adaptation and vulnerability. In: Parry, M.L., Canziani, O.F., Palutikof, J.P., van der Linden, P.J., Hanson, C.E. (eds.) Contribution of Working Group II to the Fourth Assessment Report of the Intergovernmental Panel on Climate Change. Cambridge University Press, Cambridge (2007b)

IPCC: Climate change 2013: the physical science basis. In: Stocker, T.F., Qin, D., Plattner, G.-K., Tignor, M., Allen, S.K., Boschung, J., Nauels, A., Xia, Y., Bex, V., Midgley, P.M. (eds.) Contribution of Working Group I to the Fifth Assessment Report of the Intergovernmental Panel on Climate Change. Cambridge University Press, Cambridge (2013)

Kim, B.-M., Hong, J.-Y., Jun, S.-Y., Zhang, X., Kwon, H., Kim, S.-J., Kim, J.-H., Kim, S.-W., Kim, H.-K.: Major cause of unprecedented Arctic warming in January 2016: critical role of an Atlantic windstorm. Sci. Rep. **7**, 40051 (2017). https://doi.org/10.1038/srep40051

Kobayashi, Y., Ota, Y., Harada, Y., Ebita, A., Moriya, M., Onoda, H., Onogi, K., Kamahori, H., Kobayashi, C., Endo, H., Miyaoka, K., Takahash, K.: The JRA-55 reanalysis: general specifications and basic characteristics. J. Meteor. Soc. Japan. Ser. II. **93**, 5–48 (2015). https://doi.org/10.2151/jmsj.2015-001

Lee, S.: A theory for polar amplification from a general circulation perspective. Asia-Pacific J. Atmos. Sci. **50**, 31–43 (2014). https://doi.org/10.1007/s13143-014-0024-7

Luo, D., Yao, Y., Feldstein, S.B.: Regime transition of the North Atlantic oscillation and the extreme cold event over Europe in January–February 2012. Mon. Weather Rev. **142**, 4735–4757 (2014). https://doi.org/10.1175/MWR-D-13-00234.1

Luo, B., Luo, D., Wu, L., Zhong, L., Simmonds, I.: Atmospheric circulation patterns which promote winter Arctic Sea ice decline. Environ. Res. Lett. **12**, 054017 (2017). https://doi.org/10.1088/1748-9326/aa69d0

Messori, G., Woods, C., Caballero, R.: On the drivers of wintertime temperature extremes in the high Arctic. J. Clim. **31**, 1597–1618 (2018). https://doi.org/10.1175/JCLI-D-17-0386.1

Michel, C., Rivière, G., Terray, L., Joly, B.: The dynamical link between surface cyclones, upper-tropospheric Rossby wave breaking and the life cycle of the Scandinavian blocking. Geophys. Res. Lett. **39**, L10806 (2012). https://doi.org/10.1029/2012GL051682

Orsolini, Y.J., Sorteberg, A.: Projected changes in Eurasian and Arctic summer cyclones under global warming in the Bergen climate model. Atmos. Oceanic Sci. Lett. **2**, 62–67 (2009). https://doi.org/10.1080/16742834.2009.11446776

Overland, J.E., Wang, M.: Large-scale atmospheric circulation changes are associated with the recent loss of Arctic Sea ice. Tellus A. **62**, 1–9 (2010). https://doi.org/10.1111/j.1600-0870.2009.00421.x

Park, D.-S.R., Lee, S., Feldstein, S.B.: Attribution of the recent Winter Sea ice decline over the Atlantic sector of the Arctic Ocean. J. Clim. **28**, 4027–4033 (2015a). https://doi.org/10.1175/JCLI-D-15-0042.1

Park, H.-S., Lee, S., Son, S.-W., Feldstein, S.B., Kosaka, Y.: The impact of poleward moisture and sensible heat flux on Arctic winter sea ice variability. J. Clim. **28**, 5030–5040 (2015b)

Pinto, J.G., Raible, C.C.: Past and recent changes in the North Atlantic oscillation. WIREs Clim. Change. **3**, 79–90 (2012). https://doi.org/10.1002/wcc.150

Pithan, F., Mauritsen, T.: Arctic amplification dominated by temperature feedbacks in contemporary climate models. Nat. Geosci. **7**, 181–184 (2014). https://doi.org/10.1038/ngeo2071

Rinke, A., Maturilli, M., Graham, R.M., Matthes, H., Handorf, D., Cohen, L., Hudson, S.R., Moore, J.C.: Extreme cyclone events in the Arctic: wintertime variability and trends. Environ. Res. Lett. **12**, 094006 (2017). https://doi.org/10.1088/1748-9326/aa7def

Screen, J.A., Deser, C., Simmonds, I.: Local and remote controls on observed Arctic warming. Geophys. Res. Lett. **39**, L10709 (2012). https://doi.org/10.1029/2012GL051598

Serreze, M.C., Barrett, A.P., Stroeve, J.C., Kindig, D.N., Holland, M.M.: The emergence of surface-based Arctic amplification. Cryosphere. **3**, 11–19 (2009). https://doi.org/10.5194/tc-3-11-2009

Shindell, D., Faluvegi, G.: Climate response to regional radiative forcing during the twentieth century. Nat. Geosci. **2**, 294–300 (2009). https://doi.org/10.1038/ngeo473

Simmonds, I., Rudeva, I.: A comparison of tracking methods for extreme cyclones in the Arctic basin. Tellus A. **66**, 25252 (2014). https://doi.org/10.3402/tellusa.v66.25252

Stroeve, J.C., Serreze, M.C., Holland, M.M., Kay, J.E., Malanik, J., Barrett, A.P.: The Arctic's rapidly shrinking sea ice cover: a research synthesis. Clim. Chang. **110**, 1005–1027 (2012). https://doi.org/10.1007/s10584-011-0101-1

Tamarin, T., Kaspi, Y.: The poleward motion of extratropical cyclones from a potential vorticity tendency analysis. J. Atmos. Sci. **73**, 1687–1707 (2016)

Tamarin, T., Kaspi, Y.: The poleward shift of storm tracks under global warming: a Lagrangian perspective. Geophys. Res. Lett. **44**, 10666–10674 (2017a)

Tamarin, T., Kaspi, Y.: Enhanced poleward propagation of storms under climate change. Nat. Geosci. **10**, 908–913 (2017b)

Vitart, F., Anderson, J.L., Stern, W.F.: Simulation of interannual variability of tropical storm frequency in an ensemble of GCM integrations. J. Clim. **10**, 745–760 (1997). https://doi.org/10.1175/1520-0442(1997)010<0745:SOIVOT>2.0.CO;2

Winton, M.: Amplified Arctic climate change: what does surface albedo feedback have to do with it? Geophys. Res. Lett. **33**, L03701 (2006). https://doi.org/10.1029/2005GL025244

Woods, C., Caballero, R.: The role of moist intrusions in winter Arctic warming and sea ice decline. J. Clim. **29**, 4473–4485 (2016). https://doi.org/10.1175/JCLI-D-15-0773.1

Woods, C., Caballero, R., Svensson, G.: Large-scale circulation associated with moisture intrusions into the Arctic during winter. Geophys. Res. Lett. **40**, 4717–4721 (2013). https://doi.org/10.1002/grl.50912

Zhang, X., Walsh, J.E., Zhang, J., Bhatt, U., Ikeda, M.: Climatology and interannual variability of Arctic cyclone activity: 1948–2002. J. Clim. **17**, 2300–2317 (2004). https://doi.org/10.1175/1520-0442(2004)017<2300:CAIVOA>2.0.CO;2

Zhang, X., He, J., Zhang, J., Polyakov, I., Gerdes, R., Inoue, J., Wu, P.: Enhanced poleward moisture transport and amplified northern high-latitude wetting trend. Nat. Clim. Chang. **3**, 47–51 (2013). https://doi.org/10.1038/nclimate1631